Nonlinear Dyn (2012) 70:1903–1918
DOI 10.1007/s11071-012-0582-0

ORIGINAL PAPER

New spatial curved beam and cylindrical shell elements of gradient-deficient Absolute Nodal Coordinate Formulation

Cheng Liu · Qiang Tian · Haiyan Hu

Received: 8 April 2012 / Accepted: 16 August 2012 / Published online: 8 September 2012

Abstract Based on previous studies, a new spatial curved slender-beam finite element and a new cylindrical shell finite element are proposed in the frame of gradient-deficient Absolute Nodal Coordinate Formulation (ANCF). The strain energy of the beam element is derived by using the definition of the Green–Lagrange strain tensor in continuum mechanics so that the assumption on small strain can be relaxed. By using the differential geometry and the continuum mechanics, the angle between two base vectors of a defined local coordinate frame of the cylindrical shell element is introduced into the strain energy formulations. Therefore, the new shell element can be used to model parallelogram shells. The analytical formulations of elastic forces and their Jacobian for the above two finite elements of gradient-deficient ANCF are also derived via the skills of tensor analysis. The generalized-alpha method is used to solve the huge set of system equations. Finally, four case studies including both static and dynamic problems are given to validate the proposed beam and cylindrical shell elements of gradient-deficient ANCF.

Keywords Absolute Nodal Coordinate Formulation (ANCF) · Gradient deficient · Spatial curved beam element · Cylindrical shell element

C. Liu · Q. Tian (✉) · H. Hu
MOE Key Laboratory of Dynamics and Control of Flight Vehicle, School of Aerospace Engineering, Beijing Institute of Technology, Beijing 100081, China
e-mail: tianqiang_hust@yahoo.com.cn

C. Liu
e-mail: liucheng_bit@yahoo.cn

H. Hu
e-mail: haiyan_hu@bit.edu.cn

1 Introduction

The past decade has witnessed numerous theoretical and numerical advances in the Absolute Nodal Coordinate Formulation (ANCF) for the dynamics of flexible multibody systems, initially proposed by Shabana [1], as an accurate, non-incremental finite element method to deal with the dynamics of those systems subject to both large overall motions and large deformations. The ANCF, hence, has become a benchmark in the development of dynamics of flexible multibody systems [2–4].

Many kinds of finite elements of ANCF have been proposed for modeling both large overall motion and large deformation of a constrained multibody system. These finite elements can be classified into two types according to their gradient coordinates, i.e., the fully parameterized finite elements and the gradient-deficient finite elements. For the fully parameterized finite elements, such as the spatial beam element of ANCF proposed by Shabana and Yakoub [5, 6], the plate element of ANCF proposed by Mikkola and Shabana [7], the planar shear deformable beam element

of ANCF proposed by Omar and Shabana [8] and the laminated plate element of ANCF proposed by Liu et al. [9], all the nine gradient coordinates in the spatial case or all the four gradient coordinates in the planar case are used to describe the overall motion and the deformation of a finite element. Such finite elements lead to the complete description of the element deformation, including the cross-sectional deformation of beams and plates. The corresponding fully parameterized curved elements of ANCF can also be achieved by using the isoparametric mapping method, such as the fully parameterized spatial curved beam element of ANCF proposed by Sugiyama and Suda [10]. For modeling slender or thin structures like cables, belts and membranes, many finite elements of gradient-deficient ANCF have been proposed. In these finite elements, fewer gradient coordinates are used to describe the motion of the centerline of a beam or the mid-surface of a plate/shell. For example, Mikkola et al. [11] proposed a shear deformable planar beam element of gradient-deficient ANCF with two nodes and demonstrated that the shear deformation can also be parameterized by using a vector describing the orientation of the cross section as nodal coordinates. The mass matrix of the proposed finite element, however, is no longer constant. Shabana and Maqueda [12] proposed a procedure for modeling the slope discontinuities between the gradient-deficient finite elements by using the concept of intermediate finite element coordinate system while keeping constant mass matrices.

It is also possible to generalize a planar beam element of gradient-deficient ANCF to a curved beam of the same kind. For example, Sugiyama et al. [13] studied the case of a planar beam element and eliminated the effect of strains in initially curved beam by using one-dimensional Almansi strain. Gerstmayr and Shabana [14] proposed a spatial beam element of gradient-deficient ANCF, and only used one position vector and one gradient vector as nodal coordinates for each node. Recently, Gerstmayr and Irschik [15] found that for the planar slender-beam element of ANCF proposed in [16], the use of the Green–Lagrange strain and the Piola–Kirchhoff stress of the second type brings about a strong coupling between the axial strain and the bending strain in deriving the elastic energy formulation of the element, whereas such a coupling may lead to inaccurate numerical results. Thus, they utilized both Biot strain and stress tensors in the description of elastic energy and proposed a novel method to avoid the strain coupling problems [15]. The corresponding spatial curved beam element of gradient-deficient ANCF, however, has not yet received any attention. Dmitrochenko and Pogorelov [17] developed a thin plate element of gradient-deficient ANCF in which the transverse gradients were not adopted as nodal coordinates. Furthermore, the Kirchhoff theory that they used does not account for the shear deformation. Hence, their plate element cannot be directly used to model shell structures. Furthermore, the spatial curved beam and plate elements of gradient-deficient ANCF may easily suffer from significant curvature/membrane locking due to the use of Hermite spline for shape functions. Sanborn et al. [18] named the phenomenon a Curve-Induced Distortion (CID), which can lead to the axial and membrane strain distortions in a thin plate element of gradient-deficient ANCF. To counteract CID problem, Sanborn et al. [18] proposed a Flat-Mapped Extension Modeling (FMEM) method to reduce the effect of CID through the use of a 1D Hermite polynomial kinematically linked to the 3D Hermite curve to represent the axial displacement field. However, it is still an open problem to establish any thin shell elements of gradient-deficient ANCF.

In this paper, based on the previous studies on the finite elements of gradient-deficient ANCF, especially the works by Gerstmayr and Shabana [14], Gerstmayr et al. [15] and Dmitrochenko and Pogorelov [17], a new spatial curved slender-beam element and a new thin cylindrical shell element are proposed in the frame of gradient-deficient ANCF. The remaining part of the paper is organized as follows. From the definition of Green–Lagrange strain tensor in continuum mechanics [19], the strain energy formulation for a new spatial curved slender-beam element of ANCF is derived in Sect. 2 so that the assumption on small element strains can be removed. In Sect. 3, a Cartesian coordinate frame and a curved surface coordinate frame are defined at an arbitrary point in a new cylindrical shell element of ANCF. Based on the careful analysis of element deformation, the formulation of calculating the strain energy of mid-surface is proposed. The bending strain energy of the cylindrical shell element of ANCF is also deducted by using the Weingarten's formula [20]. The angle between two base vectors of a defined curved surface coordinate frame on the element mid-surface is introduced into the formulation of element strain energy so that

the cylindrical shell element of ANCF can be used to model flexible curved parallelogram structures. In Sect. 4, the analytical expression of the elastic forces and their Jacobian for the above two finite elements of ANCF are deducted. In Sect. 5, an efficient computational strategy for solving the equations of motion is briefly introduced. Four case studies are given in Sect. 6 to testify the above results. The first case is the static test of a cantilever thin parallelogram plate. The second case is about the bending tests of a spatial curved cantilever beam and a cantilever shell. The third case is a classic example to test the performance of a cylindrical shell element, that is, an open-ended cylindrical shell subjected two opposite forces. The final case is to study the dynamics of a double pendulum composed of two parts of thin cylindrical shells. In Sect. 7, the main conclusions are drawn and the perspectives for future researches are outlined.

2 A spatial curved slender-beam element of ANCF

2.1 Longitudinal strain energy of a spatial curved slender-beam element

According to the work by Gerstmayr and Shabana [14], the nodal coordinates of a spatial curved slender-beam element of ANCF as shown in Fig. 1 can be expressed as

$$\mathbf{e} = \left[\mathbf{r}_i^{\mathrm{T}} \quad \mathbf{r}_{i,x}^{\mathrm{T}} \quad \mathbf{r}_j^{\mathrm{T}} \quad \mathbf{r}_{j,x}^{\mathrm{T}} \right]^{\mathrm{T}}. \tag{1}$$

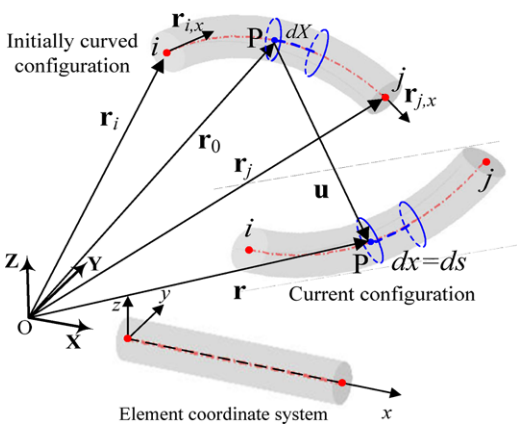

Fig. 1 A spatial curved slender-beam element in initial and current configurations

Then, the displacement of an arbitrary point P on the beam axis yields

$$\mathbf{r}(\xi) = \mathbf{S}(\xi)\mathbf{e} = \left[S_1\mathbf{I}_3 \quad S_2\mathbf{I}_3 \quad S_3\mathbf{I}_3 \quad S_4\mathbf{I}_3 \right]\mathbf{e}, \tag{2}$$

where $\mathbf{S}$ denotes the element shape function, $S_1 = 1 - 3\xi^2 + 2\xi^3$, $S_2 = l(3\xi^2 - 2\xi^3)$, $S_3 = \xi - 2\xi^2 + \xi^3$, $S_4 = l(-\xi^2 + \xi^3)$. Here, $0 \le \xi \le 1$, l is the initial arc length of the axis of the beam element.

In Fig. 1, $\mathrm{d}x$ denotes the infinitesimal arc length along the element axis in current configuration and $\mathrm{d}X$ denotes the infinitesimal arc length along the element axis in original reference configuration. According to the continuum mechanics [19], the longitudinal strain ε^l can be cast as

$$(\mathrm{d}x)^2 - (\mathrm{d}X)^2 = 2\mathrm{d}X\varepsilon^l\,\mathrm{d}X. \tag{3}$$

The square of the arc length of an infinitesimal arc segment can be further calculated, by using the infinitesimal displacement vector defined in the global coordinate frame, as

$$\begin{cases} (\mathrm{d}x)^2 = \mathrm{d}\mathbf{r}\cdot\mathrm{d}\mathbf{r} = \dfrac{\mathrm{d}\mathbf{r}}{\mathrm{d}\xi}\mathrm{d}\xi\cdot\dfrac{\mathrm{d}\mathbf{r}}{\mathrm{d}\xi}\mathrm{d}\xi \\ (\mathrm{d}X)^2 = \mathrm{d}\mathbf{r}_0\cdot\mathrm{d}\mathbf{r}_0 = \dfrac{\mathrm{d}\mathbf{r}_0}{\mathrm{d}\xi}\mathrm{d}\xi\cdot\dfrac{\mathrm{d}\mathbf{r}_0}{\mathrm{d}\xi}\mathrm{d}\xi. \end{cases} \tag{4}$$

From Eq. (4), the differentiation of the arc length of the beam axis with respect to ξ can be written as

$$\begin{cases} \mathrm{d}x = \mathrm{d}s = \left|\dfrac{\mathrm{d}\mathbf{r}}{\mathrm{d}\xi}\right|\mathrm{d}\xi \\ \mathrm{d}X = \left|\dfrac{\mathrm{d}\mathbf{r}_0}{\mathrm{d}\xi}\right|\mathrm{d}\xi. \end{cases} \tag{5}$$

Substitution of Eqs. (4) and (5) into Eq. (3), hence, gives the longitudinal strain ε_l

$$\varepsilon^l = \frac{1}{2}\left(\frac{\mathrm{d}\mathbf{r}}{\mathrm{d}\xi}\left|\frac{\mathrm{d}\mathbf{r}_0}{\mathrm{d}\xi}\right|^{-1}\cdot\frac{\mathrm{d}\mathbf{r}}{\mathrm{d}\xi}\left|\frac{\mathrm{d}\mathbf{r}_0}{\mathrm{d}\xi}\right|^{-1} - 1\right). \tag{6}$$

The value of $|\frac{\mathrm{d}\mathbf{r}_0}{\mathrm{d}\xi}|$ is equal to the initial length of the beam element in theory and can be determined by

$$\left|\frac{\mathrm{d}\mathbf{r}_0}{\mathrm{d}\xi}\right| = \left|\frac{\mathrm{d}\mathbf{S}}{\mathrm{d}\xi}\mathbf{e}_0\right|. \tag{7}$$

Therefore, the longitudinal strain energy formulation for the beam element shown in Fig. 1 can be expressed

by

$$U^l = \frac{1}{2}\int_l EA(\varepsilon^l)^2\,\mathrm{d}l, \tag{8}$$

where E is the Young's modulus of the beam material.

2.2 Bending strain energy of a spatial curved slender-beam element

According to the differential geometry [20] and Eq. (5), a Frenet coordinate frame $\boldsymbol{\alpha}$-$\boldsymbol{\beta}$-$\boldsymbol{\gamma}$ can be defined at an arbitrary point P on the axis of a spatial curved slender-beam element as shown in Fig. 2 as following:

$$\begin{cases} \boldsymbol{\alpha}(s) = \dfrac{\mathrm{d}\mathbf{r}}{\mathrm{d}s} = \mathbf{r}_\xi |\mathbf{r}_\xi|^{-1} \\ \dfrac{\mathrm{d}\boldsymbol{\alpha}(s)}{\mathrm{d}s} = \kappa(s)\boldsymbol{\beta}(s) \\ \boldsymbol{\gamma}(s) = \boldsymbol{\alpha}(s) \times \boldsymbol{\beta}(s), \end{cases} \tag{9}$$

where s is the arc coordinate along the curved element axis, $\boldsymbol{\alpha}(s)$ is the curve tangent vector at point P. The base vectors $\boldsymbol{\beta}(s)$ and $\boldsymbol{\gamma}(s)$ are called the normal and binormal vectors, respectively; $\kappa(s) = \kappa(\xi) = \frac{|\mathbf{r}_\xi \times \mathbf{r}_{\xi\xi}|}{|\mathbf{r}_\xi|^3}$ represents the curvature of the curved axis at point P, $\mathbf{r}_\xi = \frac{\mathrm{d}\mathbf{r}}{\mathrm{d}\xi}$ and $\mathbf{r}_{\xi\xi} = \frac{\mathrm{d}^2\mathbf{r}}{\mathrm{d}\xi^2}$.

From the definition of base vectors in Eq. (9), it is obvious that the plane determined by $\boldsymbol{\beta}(s)$ and $\boldsymbol{\gamma}(s)$ is always perpendicular to the tangent vector $\boldsymbol{\alpha}(s)$. Under the deformation assumption of Euler beam, it can be seen from Fig. 2 that the position vector of an arbitrary point B on the plane determined by base vectors $\boldsymbol{\beta}(s)$ and $\boldsymbol{\gamma}(s)$ in the beam element can be described

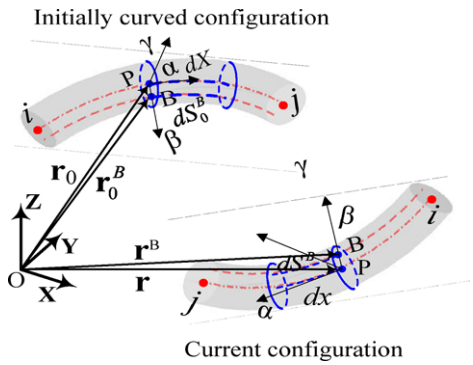

Fig. 2 The position vector of an arbitrary point on the spatial curved slender-beam element

by

$$\mathbf{r}^B = \mathbf{r} + y\boldsymbol{\beta}(s) + z\boldsymbol{\gamma}(s), \tag{10}$$

where y and z are the local coordinates defined in the Frenet coordinate frame $\boldsymbol{\alpha}$-$\boldsymbol{\beta}$-$\boldsymbol{\gamma}$.

From Eq. (9), the formulation to describe the kinematic properties of a moving particle along a curve can be expressed by

$$\begin{cases} \boldsymbol{\alpha}'(s) = \dfrac{\mathrm{d}\boldsymbol{\alpha}(s)}{\mathrm{d}s} = \kappa(\xi)\boldsymbol{\beta}(s) \\ \boldsymbol{\beta}'(s) = \dfrac{\mathrm{d}\boldsymbol{\beta}(s)}{\mathrm{d}s} = -\kappa(\xi)\boldsymbol{\alpha}(s) + \tau(s)\boldsymbol{\gamma}(s) \\ \boldsymbol{\gamma}'(s) = \dfrac{\mathrm{d}\boldsymbol{\gamma}(s)}{\mathrm{d}s} = -\tau(s)\boldsymbol{\beta}(s), \end{cases} \tag{11}$$

where $\tau(s)$ represents the torsion of the curve.

As shown in Fig. 2, according to the continuum mechanics and Eq. (10), the square of the arc length of an infinitesimal arc segment close to point B in the beam element in the current configuration can be expressed by

$$\begin{aligned} \left(\mathrm{d}s^B\right)^2 &= \mathrm{d}\mathbf{r}^B \cdot \mathrm{d}\mathbf{r}^B \\ &= \left(\frac{\mathrm{d}\mathbf{r}^B}{\mathrm{d}\xi}\,\mathrm{d}\xi\right) \cdot \left(\frac{\mathrm{d}\mathbf{r}^B}{\mathrm{d}\xi}\,\mathrm{d}\xi\right) \\ &= \left(\frac{\mathrm{d}\mathbf{r}}{\mathrm{d}\xi} + y\frac{\mathrm{d}\boldsymbol{\beta}(s)}{\mathrm{d}\xi} + z\frac{\mathrm{d}\boldsymbol{\gamma}(s)}{\mathrm{d}\xi}\right) \\ &\quad \times \left(\frac{\mathrm{d}\mathbf{r}}{\mathrm{d}\xi} + y\frac{\mathrm{d}\boldsymbol{\beta}(s)}{\mathrm{d}\xi} + z\frac{\mathrm{d}\boldsymbol{\gamma}(s)}{\mathrm{d}\xi}\right)\mathrm{d}\xi\,\mathrm{d}\xi \\ &= \left(\frac{\mathrm{d}\mathbf{r}}{\mathrm{d}\xi} + y\frac{\mathrm{d}\boldsymbol{\beta}(s)}{\mathrm{d}s}\frac{\mathrm{d}s}{\mathrm{d}\xi} + z\frac{\mathrm{d}\boldsymbol{\gamma}(s)}{\mathrm{d}\xi}\right) \\ &\quad \times \left(\frac{\mathrm{d}\mathbf{r}}{\mathrm{d}\xi} + y\frac{\mathrm{d}\boldsymbol{\beta}(s)}{\mathrm{d}s}\frac{\mathrm{d}s}{\mathrm{d}\xi} + z\frac{\mathrm{d}\boldsymbol{\gamma}(s)}{\mathrm{d}s}\frac{\mathrm{d}s}{\mathrm{d}\xi}\right)\mathrm{d}\xi\,\mathrm{d}\xi. \end{aligned} \tag{12}$$

Substituting Eqs. (5) and (11) into Eq. (12) and using the orthogonality relationships among vectors $\boldsymbol{\alpha}(s)$, $\boldsymbol{\beta}(s)$ and $\boldsymbol{\gamma}(s)$, Eq. (12) can be further written as

$$\begin{aligned} &\left(\mathrm{d}s^B\right)^2 \\ &\approx \left(\mathbf{r}_\xi \cdot \mathbf{r}_\xi + 2y\mathbf{r}_\xi \cdot \frac{\mathrm{d}\boldsymbol{\beta}(s)}{\mathrm{d}\xi} + 2z\mathbf{r}_\xi \cdot \frac{\mathrm{d}\boldsymbol{\gamma}(s)}{\mathrm{d}\xi}\right)\mathrm{d}\xi\,\mathrm{d}\xi \\ &= \left(\mathbf{r}_\xi \cdot \mathbf{r}_\xi - 2y|\mathbf{r}_\xi|^2\kappa(\xi)\right)\mathrm{d}\xi\,\mathrm{d}\xi. \end{aligned} \tag{13}$$

In Eq. (13), the higher-order terms of y and z are ignored.

Similarly, the square of the original arc length of an infinitesimal arc segment close to point B in the beam element in the initial configuration can be written as

$$\left(\mathrm{d}s_0^B\right)^2 \approx \left((\mathbf{r}_0)_\xi \cdot (\mathbf{r}_0)_\xi - 2y\left|(\mathbf{r}_0)_\xi\right|^2 \kappa_0(\xi)\right)\mathrm{d}\xi\,\mathrm{d}\xi, \tag{14}$$

where

$$(\mathbf{r}_0)_\xi = \frac{\mathrm{d}\mathbf{r}_0}{\mathrm{d}\xi}, \quad (\mathbf{r}_0)_{\xi\xi} = \frac{\mathrm{d}^2\mathbf{r}_0}{\mathrm{d}\xi^2} \quad \text{and}$$
$$\kappa_0(\xi) = \frac{|(\mathbf{r}_0)_\xi \times (\mathbf{r}_0)_{\xi\xi}|}{|(\mathbf{r}_0)_\xi|^3}.$$

From the definition of the Green–Lagrange strain tensor in continuum mechanics [19], the strain of infinitesimal segment of the beam element close to B can be obtained by

$$\left(\mathrm{d}s^B\right)^2 - \left(\mathrm{d}S_0^B\right)^2 = 2\mathrm{d}S_0^B \varepsilon^B \mathrm{d}S_0^B. \tag{15}$$

Substituting Eqs. (13) and (14) into Eq. (15), the strain at an arbitrary point in the beam element can be expressed by

$$\begin{aligned}\varepsilon^B &= \frac{\mathbf{r}_\xi \cdot \mathbf{r}_\xi - (\mathbf{r}_0)_\xi \cdot (\mathbf{r}_0)_\xi - 2y|\mathbf{r}_\xi|^2\kappa(\xi) + 2y|(\mathbf{r}_0)_\xi|^2\kappa_0(\xi)}{2(|(\mathbf{r}_0)_\xi|^2 - 2y|(\mathbf{r}_0)_\xi|^2\kappa_0(\xi))} \\ &\approx \frac{\mathbf{r}_\xi \cdot \mathbf{r}_\xi - (\mathbf{r}_0)_\xi \cdot (\mathbf{r}_0)_\xi - 2y|\mathbf{r}_\xi|^2\kappa(\xi) + 2y|(\mathbf{r}_0)_\xi|^2\kappa_0(\xi)}{2|(\mathbf{r}_0)_\xi|^2} \\ &= \varepsilon^l + \varepsilon^\kappa. \end{aligned} \tag{16}$$

From Eq. (16), the strain function only depends on the local y coordinates along the direction of $\boldsymbol{\beta}(s)$ describing the element bending. The total strain is the summation of longitudinal strain ε^l and bending strain ε^k, where the pure bending strain ε^k can be written as

$$\begin{aligned}\varepsilon^\kappa &= \frac{y}{|(\mathbf{r}_0)_\xi|^2}\left(-|\mathbf{r}_\xi|^2\kappa(s) + \left|(\mathbf{r}_0)_\xi\right|^2\kappa_0(s)\right) \\ &= \frac{y}{|(\mathbf{r}_0)_\xi|^2}\left(\bar{\kappa}_0(\xi) - \bar{\kappa}(\xi)\right), \end{aligned} \tag{17}$$

where $\bar{\kappa}(\xi) = \bar{\kappa}(s) = \frac{|\mathbf{r}_\xi \times \mathbf{r}_{\xi\xi}|}{|\mathbf{r}_\xi|}$ and $\bar{\kappa}_0(\xi) = \bar{\kappa}_0(s) = \frac{|(\mathbf{r}_0)_\xi \times (\mathbf{r}_0)_{\xi\xi}|}{|(\mathbf{r}_0)_\xi|}$. Thus, the pure bending strain energy can be written as

$$\begin{aligned}U^\kappa &= \frac{1}{2}\iiint_{V_0} E\varepsilon^\kappa\varepsilon^\kappa\,\mathrm{d}V_0 \\ &= \frac{1}{2}\iiint_{V_0} Ey^2\left(\frac{\bar{\kappa}_0(s) - \bar{\kappa}(s)}{|(\mathbf{r}_0)_\xi|^2}\right)^2\mathrm{d}V_0 \\ &= \frac{1}{2}\int_l EI\frac{1}{|(\mathbf{r}_0)_\xi|^4}\left[\bar{\kappa}(\xi) - \bar{\kappa}_0(\xi)\right]^2\mathrm{d}l. \end{aligned} \tag{18}$$

Finally, the total strain energy of a beam element can be obtain by

$$\begin{aligned}U &= U^l + U^\kappa \\ &= \frac{1}{2}\int_l\left[EA\left(\varepsilon^l\right)^2 + \frac{EI}{|(\mathbf{r}_0)_\xi|^4}(\bar{\kappa} - \bar{\kappa}_0)^2\right]\mathrm{d}l. \end{aligned} \tag{19}$$

In some previous studies on the spatial curved slender-beam element of ANCF, the total elastic energy formulation is written as [14]

$$U = \frac{1}{2}\int_l\left[EA\left(\varepsilon^l\right)^2 + EI\kappa^2(\xi)\right]\mathrm{d}l. \tag{20}$$

By a careful comparison between Eqs. (19) and (20) it is possible to see that the terms of the longitudinal energy are identical. However, the formulations of bending energy are slightly different. From Eq. (15) it can be seen that the definition of the Green–Lagrange strain is used to derive the formulation of bending strain, whereas for Eq. (20) the definition of engineering strain is used to deduct the bending strain energy [14]. In fact, only under the assumption on small strain in the beam element, the Green–Lagrange strain tensor can degenerate into the engineering strain [19]. Therefore, the new spatial curved slender-beam element of ANCF can be used in the dynamic analysis of very flexible beams undergoing large strains. Furthermore, Gerstmayr and Irschik [15] carefully discussed the inaccuracy problem of Eq. (20) and found that using the Green–Lagrange strain and the Piola–Kirchhoff stress of the second type may bring about a strong coupling between the axis strain and the bending strain in deriving the elastic energy formulation of the element. In order to decouple the coupled strain terms in the strain energy, they utilized the Biot strain tensor and the Biot stress tensor in the deduction of element elastic energy.

In fact, the expression of elastic energy of the spatial element presented in this paper can also be degenerated into the corresponding formulation derived by Gerstmayr and Irschik [15]. Based on Eq. (12), for the planar beam element of ANCF, the square of the arc length of an infinitesimal arc segment close to point B in the beam element in the current configuration can be expressed by

$$\begin{aligned}\left(\mathrm{d}s^B\right)^2 &= \mathrm{d}\mathbf{r}^B \cdot \mathrm{d}\mathbf{r}^B \\ &= \left(\frac{\mathrm{d}\mathbf{r}}{\mathrm{d}\xi} + y\frac{\mathrm{d}\boldsymbol{\beta}(s)}{\mathrm{d}\xi}\right) \cdot \left(\frac{\mathrm{d}\mathbf{r}}{\mathrm{d}\xi} + y\frac{\mathrm{d}\boldsymbol{\beta}(s)}{\mathrm{d}\xi}\right) \mathrm{d}\xi\,\mathrm{d}\xi \\ &= \left(|\mathbf{r}_\xi|^2 - 2y|\mathbf{r}_\xi|^2\kappa(\xi) + y^2|\mathbf{r}_\xi|^2\kappa^2(\xi)\right)\mathrm{d}\xi\,\mathrm{d}\xi. \end{aligned} \tag{21}$$

Thus, the strain at an arbitrary point of the beam element described by Eq. (16) can be degenerated to

$$\begin{aligned}\varepsilon^B &= \frac{(|\mathbf{r}_\xi|^2 - 2y|\mathbf{r}_\xi|^2\kappa(\xi) + y^2|\mathbf{r}_\xi|^2\kappa^2(\xi)) - |\mathbf{r}_{0\xi}|^2}{2|\mathbf{r}_{0\xi}|^2} \\ &= \frac{|\mathbf{r}_x|^2 - 1 - 2y|\mathbf{r}_x|^2\kappa(\xi) + y^2|\mathbf{r}_x|^2\kappa^2(\xi)}{2} \\ &= \frac{|\mathbf{r}_x|^2 - 1 - 2y|\mathbf{r}_x|K + y^2K^2}{2} \\ &\approx \frac{|\mathbf{r}_x|^2 - 1 - 2y|\mathbf{r}_x|K}{2}, \end{aligned} \tag{22}$$

where the term $K = \frac{|\mathbf{r}_x \times \mathbf{r}_{xx}|}{|\mathbf{r}_x|^2}$ is a material measure of curvature. It can be clearly concluded that if the infinitesimal term "y^2" is not ignored, Eq. (22) will be identical to Eq. (75) in the work by Gerstmayr and Irschik [15]. It should be also noted that based on the definitions of both Biot stress tensor and Biot strain tensor, more accurate elastic energy formulation can be deducted based on this work. The readers interested in the details of the deduction procedures are referred to the work by Gerstmayr and Irschik [15].

3 A thin cylindrical shell element of ANCF

3.1 Mid-surface strain energy of a thin cylindrical shell element

Previous studies on the thin structures in the frame of ANCF have focused on the rectangle plate elements. Among them, Dmitrochenko and Pogorelov [17] proposed a thin plate element of ANCF. Based on their work, this section presents a thin cylindrical shell element of ANCF so as to deal with more complicated problems of thin structures. From Fig. 3, the displacement of an arbitrary point $\mathrm{P}(\xi, \eta)$ on the mid-surface of a thin shell element of ANCF can be expressed by

$$\mathbf{r}_0(\xi, \eta) = \mathbf{S}(\xi, \eta)\mathbf{e}_0, \tag{23}$$

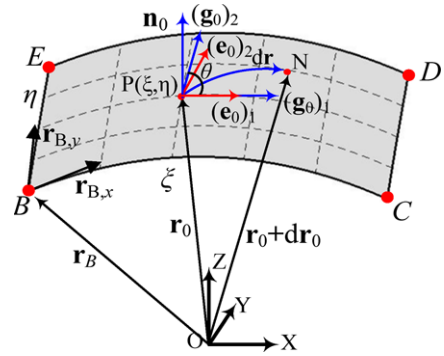

Fig. 3 Mid-surface and nodes of a thin shell element of ANCF

where $\mathbf{S}$ is the element shape function that can be found in the work by Dmitrochenko and Pogorelov [17], $0 \le \xi \le 1$ and $0 \le \eta \le 1$ can be regarded as the canonical parameters of the mid-surface of the thin shell element.

As shown in Fig. 3, a local curved surface coordinate frame $(\mathbf{g}_0)_1$-$(\mathbf{g}_0)_2$-$\mathbf{n}_0$ and a Cartesian coordinate frame $(\mathbf{e}_0)_1$-$(\mathbf{e}_0)_2$-$(\mathbf{e}_0)_3$ are defined at an arbitrary point $\mathrm{P}(\xi, \eta)$ for further deformation analysis of the thin shell element of ANCF. For the local curved surface coordinate frame $(\mathbf{g}_0)_1$-$(\mathbf{g}_0)_2$-$\mathbf{n}_0$, one has

$$\begin{cases} (\mathbf{g}_0)_1 = (\mathbf{r}_0)_\xi = \dfrac{\partial \mathbf{r}_0}{\partial \xi} \\ (\mathbf{g}_0)_2 = (\mathbf{r}_0)_\eta = \dfrac{\partial \mathbf{r}_0}{\partial \eta} \\ \mathbf{n}_0 = \dfrac{(\mathbf{g}_0)_1 \times (\mathbf{g}_0)_2}{|(\mathbf{g}_0)_1 \times (\mathbf{g}_0)_2|}. \end{cases} \tag{24}$$

From Fig. 3, the tangent plane at an arbitrary point $\mathrm{P}(\xi, \eta)$ on the mid-surface of the shell element can be defined by two tangent base vectors $\mathbf{g}_1$ and $\mathbf{g}_2$.

The unit base vectors, $(\mathbf{e}_0)_1$, $(\mathbf{e}_0)_2$ and $(\mathbf{e}_0)_3$, of the local Cartesian coordinate frame are defined as follows:

$$\begin{aligned} &(\mathbf{e}_0)_1 = \frac{(\mathbf{g}_0)_1}{|(\mathbf{g}_0)|}, \qquad (\mathbf{e}_0)_3 = \mathbf{n}_0, \\ &(\mathbf{e}_0)_2 = (\mathbf{e}_0)_3 \times (\mathbf{e}_0)_1. \end{aligned} \tag{25}$$

Let point $\mathrm{N}(\xi + \mathrm{d}\xi, \eta + \mathrm{d}\eta)$ be a point very close to point $\mathrm{P}(\xi, \eta)$ on the mid-surface of the shell element. From Fig. 4, the infinitesimal arc segment $\mathrm{d}\mathbf{r}_0$ on the mid-surface of the shell element can be decomposed in the local curved surface coordinate frame and the Cartesian coordinate frame in Eq. (26), respectively

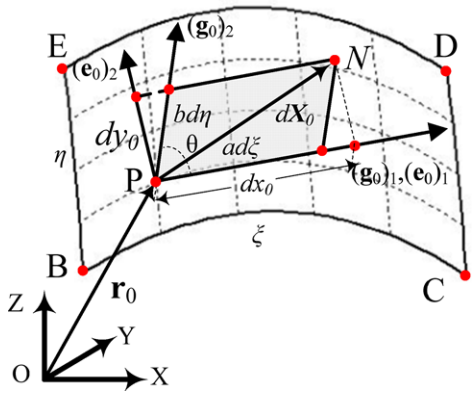

Fig. 4 Schematic view of relationship between the two local coordinate frames for a thin shell element

$$\mathrm{d}\mathbf{r}_0 = (\mathbf{g}_0)_{i'}\,\mathrm{d}\chi^{i'} = (\mathbf{e}_0)_j\,\mathrm{d}x^j, \tag{26}$$

in which $\chi^1 = \xi$, $\chi^2 = \eta$, $x^1 = x_0$, $x^2 = y_0$. Furthermore, the relationship between two covariance base vectors of the local coordinate frames $(\mathbf{g}_0)_1$-$(\mathbf{g}_0)_2$-$\mathbf{n}_0$ and $(\mathbf{e}_0)_1$-$(\mathbf{e}_0)_2$-$(\mathbf{e}_0)_3$ can be obtained by [23]

$$(\mathbf{g}_0)_{i'} = \beta_{i'}{}^{j}(\mathbf{e}_0)_j, \tag{27}$$

where $\beta_{i'}{}^{j} = (\mathbf{g}_0)_{i'}(\mathbf{e}_0)_j$ is called the coefficient of covariant transformation. Therefore, the contravariance components $\mathrm{d}\chi^{i'}$ in local coordinate frame $(\mathbf{g}_0)_1$-$(\mathbf{g}_0)_2$-$\mathbf{n}_0$ can be expressed by

$$\mathrm{d}\chi^{i'} = \beta^{i'}{}_{k}\mathrm{d}x^k, \tag{28}$$

where $\beta^{i'}{}_{k}$ is called the coefficient of contravariance transformation and satisfies $\beta^{i'}{}_{k}\beta_{i'}{}^{j} = \delta_k^j$. In this particular example, the relationship between the two local coordinate frames $\mathbf{g}_1$-$\mathbf{g}_2$-$\mathbf{n}$ and $\mathbf{e}_1$-$\mathbf{e}_2$-$\mathbf{e}_3$ can be obtained:

$$\begin{aligned}\begin{bmatrix}\mathrm{d}\xi\\ \mathrm{d}\eta\end{bmatrix} &= \begin{bmatrix}(\mathbf{g}_0)_1(\mathbf{e}_0)_1 & (\mathbf{g}_0)_1(\mathbf{e}_0)_2\\ (\mathbf{g}_0)_2(\mathbf{e}_0)_1 & (\mathbf{g}_0)_2(\mathbf{e}_0)_2\end{bmatrix}^{-\mathrm{T}}\begin{bmatrix}\mathrm{d}x_0\\ \mathrm{d}y_0\end{bmatrix}\\ &= \begin{bmatrix}\frac{1}{a} & -\frac{\cot(\theta)}{a}\\ 0 & \frac{\csc(\theta)}{b}\end{bmatrix}\begin{bmatrix}\mathrm{d}x_0\\ \mathrm{d}y_0\end{bmatrix}\\ &= \mathbf{T}\,\mathrm{d}\mathbf{X}_0,\end{aligned} \tag{29}$$

where a and b denote the arc length of element edges BC and BE in the initial configuration, respectively, and θ represents the angle between the two base vectors $(\mathbf{g}_0)_1$ and $(\mathbf{g}_0)_2$.

$$\mathbf{T} = \begin{bmatrix}\frac{1}{a} & -\frac{\cot(\theta)}{a}\\ 0 & \frac{\csc(\theta)}{b}\end{bmatrix}$$

denotes the transformation matrix between the vector $[\,\mathrm{d}\xi\ \mathrm{d}\eta\,]^{\mathrm{T}}$ and the vector $\mathrm{d}\mathbf{X}_0 = [\,\mathrm{d}x_0\ \mathrm{d}y_0\,]^{\mathrm{T}}$.

As shown in Fig. 3, the square of the arc length of the infinitesimal arc segment $\mathrm{d}s_0$ on the mid-surface of the shell element in the reference configuration can be approximated by

$$\begin{aligned}(\mathrm{d}s_0)^2 &= \mathrm{d}\mathbf{r}_0\cdot\mathrm{d}\mathbf{r}_0 = \mathrm{d}\mathbf{X}_0\cdot\mathrm{d}\mathbf{X}_0\\ &= \big((\mathbf{g}_0)_1\,\mathrm{d}\xi + (\mathbf{g}_0)_2\,\mathrm{d}\eta\big)\cdot\big((\mathbf{g}_0)_1\,\mathrm{d}\xi + (\mathbf{g}_0)_2\,\mathrm{d}\eta\big)\\ &= \begin{bmatrix}\mathrm{d}\xi & \mathrm{d}\eta\end{bmatrix}\begin{bmatrix}(g_0)_{11} & (g_0)_{12}\\ (g_0)_{12} & (g_0)_{22}\end{bmatrix}\begin{bmatrix}\mathrm{d}\xi\\ \mathrm{d}\eta\end{bmatrix}\end{aligned} \tag{30}$$

where $(\mathbf{g}_0)_1 = \frac{\partial\mathbf{r}_0}{\partial\xi}$, $(\mathbf{g}_0)_2 = \frac{\partial\mathbf{r}_0}{\partial\eta}$, $(g_0)_{\alpha\beta} = (g_0)_\alpha\cdot(g_0)_\beta$ ($\alpha = 1, 2$ and $\beta = 1, 2$) is the coefficient of the first quadratic fundamental form of the mid-surface of the shell element [21].

Similarly, the square of the arc length of the infinitesimal arc segment $\mathrm{d}s$ on the mid-surface of the shell element in the current configuration can be calculated by

$$(\mathrm{d}s)^2 = \mathrm{d}\mathbf{r}\cdot\mathrm{d}\mathbf{r} = \begin{bmatrix}\mathrm{d}\xi & \mathrm{d}\eta\end{bmatrix}\begin{bmatrix}g_{11} & g_{12}\\ g_{12} & g_{22}\end{bmatrix}\begin{bmatrix}\mathrm{d}\xi\\ \mathrm{d}\eta\end{bmatrix}, \tag{31}$$

where $g_{\alpha\beta} = g_\alpha\cdot g_\beta$ ($\alpha = 1, 2$ and $\beta = 1, 2$).

From Eqs. (30) and (31), the following relations can be also obtained:

$$\begin{aligned}&(\mathrm{d}s)^2 - (\mathrm{d}s_0)^2\\ &= \begin{bmatrix}\mathrm{d}\xi & \mathrm{d}\eta\end{bmatrix}\left(\begin{bmatrix}g_{11} & g_{12}\\ g_{12} & g_{22}\end{bmatrix}\right.\\ &\quad\left.-\begin{bmatrix}(g_0)_{11} & (g_0)_{12}\\ (g_0)_{12} & (g_0)_{22}\end{bmatrix}\right)\begin{bmatrix}\mathrm{d}\xi\\ \mathrm{d}\eta\end{bmatrix}.\end{aligned} \tag{32}$$

According to the continuum mechanics and considering Eq. (29), the Green–Lagrange strain of the mid-surface of the shell element can be written as

$$\begin{aligned}\boldsymbol{\varepsilon}^{\mathrm{mid}} &= \frac{1}{2}\mathbf{T}^{\mathrm{T}}\left(\begin{bmatrix}g_{11} & g_{12}\\ g_{12} & g_{22}\end{bmatrix} - \begin{bmatrix}(g_0)_{11} & (g_0)_{12}\\ (g_0)_{12} & (g_0)_{22}\end{bmatrix}\right)\mathbf{T}\\ &= \begin{bmatrix}\boldsymbol{\varepsilon}_{11} & \boldsymbol{\varepsilon}_{12}\\ \boldsymbol{\varepsilon}_{12} & \boldsymbol{\varepsilon}_{22}\end{bmatrix}.\end{aligned} \tag{33}$$

Therefore, the mid-surface strain energy of the shell element can be finally written as

$$U^{\text{mid}} = \frac{1}{2}\int_{V_0} \left(\boldsymbol{\varepsilon}^{\text{mid}}\right)^{\mathrm{T}} \mathbf{E}\left(\boldsymbol{\varepsilon}^{\text{mid}}\right) \mathrm{d}V_0, \tag{34}$$

where $\mathbf{E}$ is the elastic tensor of the fourth order for plane stress problem.

3.2 Bending strain energy of a thin cylindrical shell element

Figure 5 gives a scaled view of an arbitrary layer of the thin shell element of ANCF. Here, the nodes are still defined on the mid-surface π of the shell element. Based on the Kirchhoff theory of thin shells, the global location of an arbitrary point P′ on the outer surface π^z of the shell element can be determined as

$$\mathbf{r}^z = \mathbf{r}(\xi, \eta) + z\mathbf{n}(\xi, \eta), \tag{35}$$

where $\mathbf{r}$ indicates the location of the corresponding point P(ξ, η) on the mid-surface π and $\mathbf{n}$ is the unit normal vector of the mid-surface at this point.

Then, a tangent plane of the mid-surface at point P′(ξ, η) can be defined by two vectors $\mathbf{g}_1^z$ and $\mathbf{g}_2^z$, as

$$\begin{cases} \mathbf{g}_1^z = \dfrac{\partial \mathbf{r}(\xi,\eta)}{\partial \xi} + z\dfrac{\partial \mathbf{n}(\xi,\eta)}{\partial \xi} \\ \mathbf{g}_2^z = \dfrac{\partial \mathbf{r}(\xi,\eta)}{\partial \eta} + z\dfrac{\partial \mathbf{n}(\xi,\eta)}{\partial \eta}. \end{cases} \tag{36}$$

According to Weingarten's formula in differential geometry [20], the derivative of the normal vector $\mathbf{n}$ with respect to ξ and η can be written as

$$\frac{\partial \mathbf{n}}{\partial \chi^\beta} = -\zeta_\beta^{\ \gamma}\mathbf{g}_\gamma = -\zeta_{\beta\alpha}(g_{\alpha\gamma})^{-1}\mathbf{g}_\gamma, \quad (\alpha = 1,2;\ \beta = 1,2;\ \gamma = 1,2), \tag{37}$$

where $\zeta_{\beta\alpha} = \frac{\partial^2 \mathbf{r}}{\partial \chi^\alpha \partial \chi^\beta} \cdot \mathbf{n}$ $(\chi^1 = \xi, \chi^2 = \eta)$ is the coefficient of the second quadratic fundamental form of the mid-surface of the shell element [21].

Then, the square of the arc length of the infinitesimal arc segment $\mathrm{d}s^z$ on the outer surface π^z can be calculated by

$$\begin{aligned} \mathrm{d}\left(s^z\right)^2 &= \mathrm{d}\mathbf{r}^z \cdot \mathrm{d}\mathbf{r}^z = \left(\mathbf{g}_1^z\,\mathrm{d}\xi + \mathbf{g}_2^z\,\mathrm{d}\eta\right)\cdot\left(\mathbf{g}_1^z\,\mathrm{d}\xi + \mathbf{g}_2^z\,\mathrm{d}\eta\right) \\ &= \begin{bmatrix}\mathrm{d}\xi & \mathrm{d}\eta\end{bmatrix}\begin{bmatrix} g_{11}^z & g_{12}^z \\ g_{12}^z & g_{22}^z \end{bmatrix}\begin{bmatrix}\mathrm{d}\xi \\ \mathrm{d}\eta\end{bmatrix}. \end{aligned} \tag{38}$$

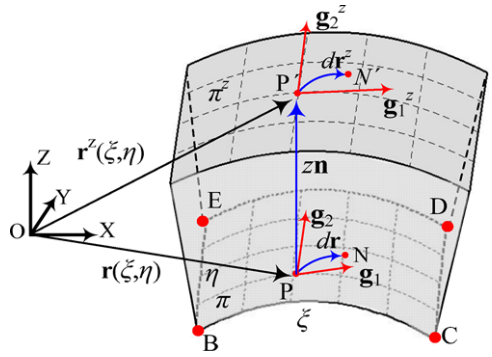

Fig. 5 Scaled view of an arbitrary layer in a thin shell element of ANCF

Hence, the square of the length of an infinitesimal segment on the surface above the mid-surface in the reference can be expressed by

$$\begin{aligned} \mathrm{d}\left(s_0^z\right)^2 &= \mathrm{d}\mathbf{r}_0^z \cdot \mathrm{d}\mathbf{r}_0^z \\ &= \begin{bmatrix}\mathrm{d}\xi & \mathrm{d}\eta\end{bmatrix}\begin{bmatrix} (g_0)_{11}^z & (g_0)_{12}^z \\ (g_0)_{12}^z & (g_0)_{22}^z \end{bmatrix}\begin{bmatrix}\mathrm{d}\xi \\ \mathrm{d}\eta\end{bmatrix}. \end{aligned} \tag{39}$$

Similarly to the procedures described by Eqs. (16) and (30)–(32), the Green–Lagrange strain of an infinitesimal arc segment of the outer surface π^z can be obtained by

$$\boldsymbol{\varepsilon} \approx \frac{1}{2}\mathbf{T}^{\mathrm{T}}\begin{bmatrix} g_{11}^z - (g_0)_{11}^z & g_{12}^z - (g_0)_{12}^z \\ g_{12}^z - (g_0)_{12}^z & g_{22}^z - (g_0)_{22}^z \end{bmatrix}\mathbf{T}, \tag{40}$$

where $(\mathbf{g}_0^z)_1 = \frac{\partial \mathbf{r}_0^z}{\partial \xi}$, $(\mathbf{g}_0^z)_2 = \frac{\partial \mathbf{r}_0^z}{\partial \eta}$ and $(g_0^z)_{\alpha\beta} = (\mathbf{g}_0^z)_\alpha \cdot (\mathbf{g}_0^z)_\beta$.

Substituting Eqs. (35)–(37) into Eq. (40) and ignoring the higher-order terms of z, the strain tensor can be written as

$$\boldsymbol{\varepsilon} \approx \boldsymbol{\varepsilon}^{\text{mid}} + \boldsymbol{\varepsilon}^{\kappa}, \tag{41}$$

where $\boldsymbol{\epsilon}^{\text{mid}}$ is the mid-surface strain formulated by using Eq. (27), $\boldsymbol{\epsilon}^{\kappa}$ denotes the bending strain of the shell element and can be further cast as

$$\boldsymbol{\varepsilon}^{\kappa} = -z\mathbf{T}^{\mathrm{T}}(\boldsymbol{\kappa} - \boldsymbol{\kappa}_0)\mathbf{T}, \tag{42}$$

where

$$\begin{cases} \boldsymbol{\kappa} = \begin{bmatrix} k_{11} & k_{12} \\ k_{12} & k_{22} \end{bmatrix} = \begin{bmatrix} \frac{\partial^2 \mathbf{r}}{\partial \xi^2}\cdot\mathbf{n} & \frac{\partial^2 \mathbf{r}}{\partial \xi \partial \eta}\cdot\mathbf{n} \\ \frac{\partial^2 \mathbf{r}}{\partial \xi \partial \eta}\cdot\mathbf{n} & \frac{\partial^2 \mathbf{r}}{\partial \eta^2}\cdot\mathbf{n} \end{bmatrix} \\ \boldsymbol{\kappa}_0 = \begin{bmatrix} (k_0)_{11} & (k_0)_{12} \\ (k_0)_{12} & (k_0)_{22} \end{bmatrix} = \begin{bmatrix} \frac{\partial^2 \mathbf{r}_0}{\partial \xi^2}\cdot\mathbf{n} & \frac{\partial^2 \mathbf{r}_0}{\partial \xi \partial \eta}\cdot\mathbf{n} \\ \frac{\partial^2 \mathbf{r}_0}{\partial \xi \partial \eta}\cdot\mathbf{n} & \frac{\partial^2 \mathbf{r}_0}{\partial \eta^2}\cdot\mathbf{n} \end{bmatrix}. \end{cases} \tag{43}$$

Thus, the bending strain energy can be expressed by

$$U^{\kappa} = \frac{1}{2}\int_{V_0} \left(\boldsymbol{\varepsilon}^{\kappa}\right)^{\mathrm{T}} \mathbf{E}\boldsymbol{\varepsilon}^{\kappa}\, \mathrm{d}V_0. \tag{44}$$

Finally, according to Eqs. (34) and (44), the total strain energy of the shell element can be written as

$$\begin{aligned} U &= U^{\kappa} + U^{\mathrm{mid}} \\ &= \frac{1}{2}\int_{V_0} \left[\left(\boldsymbol{\varepsilon}^{\mathrm{mid}}\right)^{\mathrm{T}} \mathbf{E}\left(\boldsymbol{\varepsilon}^{\mathrm{mid}}\right) + \left(\boldsymbol{\varepsilon}^{\kappa}\right)^{\mathrm{T}} \mathbf{E}\boldsymbol{\varepsilon}^{\kappa}\right] \mathrm{d}V_0. \end{aligned} \tag{45}$$

It is easy to see that if the initial configuration of the shell element is flat and rectangle, Eq. (42) for the bending stain will degenerate into the previously proposed formulation [19] as

$$\begin{aligned} \boldsymbol{\varepsilon}^{\kappa} &= -z \begin{bmatrix} 1/a & 0 \\ 0 & 1/b \end{bmatrix}^{\mathrm{T}} \begin{bmatrix} \frac{\partial^2 \mathbf{r}}{\partial \xi^2}\cdot\mathbf{n} & \frac{\partial^2 \mathbf{r}}{\partial \xi \partial \eta}\cdot\mathbf{n} \\ \frac{\partial^2 \mathbf{r}}{\partial \xi \partial \eta}\cdot\mathbf{n} & \frac{\partial^2 \mathbf{r}}{\partial \eta^2}\cdot\mathbf{n} \end{bmatrix} \\ &\quad \times \begin{bmatrix} 1/a & 0 \\ 0 & 1/b \end{bmatrix} \\ &= -z \begin{bmatrix} \frac{\partial^2 \mathbf{r}}{\partial x^2}\cdot\mathbf{n} & \frac{\partial^2 \mathbf{r}}{\partial x \partial y}\cdot\mathbf{n} \\ \frac{\partial^2 \mathbf{r}}{\partial x \partial y}\cdot\mathbf{n} & \frac{\partial^2 \mathbf{r}}{\partial y^2}\cdot\mathbf{n} \end{bmatrix}. \end{aligned} \tag{46}$$

Besides, the formulations of cylindrical shell element of ANCF proposed in this work can be directly extended to the spherical shell element of ANCF in further works.

4 Elastic forces and their Jacobian of beam and cylindrical shell elements

4.1 Formulations for a spatial curved slender-beam element of ANCF

Once the formulations of the element strain energy (Eqs. (19) and (45)) are deducted, the elastic forces $\mathbf{F}^{\mathrm{e}}$ of the two finite elements and their Jacobian $\mathbf{J}$ can be further derived. For the spatial curved slender-beam element of ANCF presented in Sect. 2, according to Eq. (19), the elastic force of the beam element can be expressed by

$$\mathbf{F}^{\mathrm{e}} = \frac{\partial U^{l}}{\partial \mathbf{e}} + \frac{\partial U^{\kappa}}{\partial \mathbf{e}} = \mathbf{Q}^{l} + \mathbf{Q}^{k}. \tag{47}$$

The elastic force associated with the longitudinal strain energy $\mathbf{Q}^{l}$ can be obtained by using a computationally efficient method proposed by Liu et al. [9]. However, this method cannot be directly used to evaluate the elastic force $\mathbf{Q}^{k}$ associated with the bending strain energy since the nodal coordinates exist in the denominator term of the bending strain energy given in Eq. (18).

Substituting Eq. (18) into Eq. (47), the elastic force associated with the bending strain energy of the beam element can be written as

$$\mathbf{Q}^{\kappa} = \frac{\partial U^{\kappa}}{\partial \mathbf{e}} = EI\int_{l} \frac{\bar{\kappa} - \bar{\kappa}_0}{|(\mathbf{r}_0)_{\xi}|^4} \frac{\partial \bar{\kappa}}{\partial \mathbf{e}}\, \mathrm{d}l. \tag{48}$$

Accordingly, the Jacobian of the elastic force can be obtained as

$$\begin{aligned} \mathbf{J}^{\kappa} &= \frac{\partial \mathbf{Q}^{\kappa}}{\partial \mathbf{e}} \\ &= EI\int_{l} \frac{1}{|(\mathbf{r}_0)_{\xi}|^4} \left[(\bar{\kappa} - \bar{\kappa}_0)\frac{\partial^2 \bar{\kappa}}{\partial \mathbf{e}^2} + \frac{\partial \bar{\kappa}}{\partial \mathbf{e}}\frac{\partial \bar{\kappa}}{\partial \mathbf{e}}\right] \mathrm{d}l. \end{aligned} \tag{49}$$

In order to enhance the computational efficiency, Eq. (2) can be rewritten as [22]

$$\mathbf{r} = \bar{\mathbf{e}}\bar{\mathbf{S}}, \tag{50}$$

where $\bar{\mathbf{e}} = [\,\mathbf{r}_i\ \mathbf{r}_{i,x}\ \mathbf{r}_j\ \mathbf{r}_{j,x}\,]$ and $\bar{\mathbf{S}} = [\,S_1\ S_2\ S_3\ S_4\,]^{\mathrm{T}}$. As can be seen from Eqs. (48) and (49), two partial derivate terms $\frac{\partial \bar{\kappa}}{\partial \mathbf{e}}$ and $\frac{\partial^2 \bar{\kappa}}{\partial \mathbf{e}^2}$ have to be evaluated in order to compute the elastic forces and their Jacobian. However, Eq. (17) indicates that it is quite difficult to directly calculate the above partial derivate terms. In fact, the results of the above two partial derivate terms can still be obtained by using the relations as follows:

$$\frac{\partial \bar{\kappa}}{\partial \mathbf{e}} = \frac{1}{2\bar{\kappa}}\frac{\partial \bar{\kappa}^2}{\partial \mathbf{e}}, \tag{51}$$

$$\frac{\partial^2 \bar{\kappa}}{\partial \mathbf{e}^2} = -\frac{1}{4\bar{\kappa}^3}\frac{\partial \bar{\kappa}^2}{\partial \mathbf{e}}\frac{\partial \bar{\kappa}^2}{\partial \mathbf{e}} + \frac{1}{2\bar{\kappa}}\frac{\partial^2 \bar{\kappa}^2}{\partial \mathbf{e}^2}. \tag{52}$$

From the formulation of $\bar{\kappa}(\xi)$ described by Eq. (17), $\bar{\kappa}^2$ can be calculated by

$$\begin{aligned} \bar{\kappa}^2 &= \frac{\epsilon_{ijk}(\mathbf{r}_{\xi})_i(\mathbf{r}_{\xi\xi})_j\epsilon_{rsk}(\mathbf{r}_{\xi})_r(\mathbf{r}_{\xi\xi})_s}{(\mathbf{r}_{\xi})_t(\mathbf{r}_{\xi})_t} \\ &= \frac{(\delta_r^i\delta_s^j - \delta_s^i\delta_r^j)(\mathbf{r}_{\xi})_i(\mathbf{r}_{\xi\xi})_j(\mathbf{r}_{\xi})_r(\mathbf{r}_{\xi\xi})_s}{(\mathbf{r}_{\xi})_t(\mathbf{r}_{\xi})_t} \\ &= (\mathbf{r}_{\xi\xi})_s(\mathbf{r}_{\xi\xi})_s - \frac{((\mathbf{r}_{\xi\xi})_r(\mathbf{r}_{\xi})_r)^2}{(\mathbf{r}_{\xi})_t(\mathbf{r}_{\xi})_t}, \end{aligned} \tag{53}$$

where ϵ denotes the Eddington tensor [23], and the subscripts in Eq. (53) must satisfy the conditions $i = 1$–3; $j = 1$–3; $k = 1$–3; $r = 1$–3; $s = 1$–3; $t = 1$–3.

Using Eqs. (51)–(53) and performing some complicated mathematic manipulations, the final formulation describing the elastic forces associated with the bending strain energy can be expressed by

$$\mathbf{Q}^{\kappa} = \frac{EI}{2}\int_l \frac{\bar{\kappa}-\bar{\kappa}_0}{\bar{\kappa}\left|(\mathbf{r}_0)_\xi\right|^4}\bar{\mathbf{e}}\cdot\boldsymbol{\Psi}_1\,\mathrm{d}l \tag{54}$$

where $\boldsymbol{\Psi}_1 = 2\mathbf{C} - \frac{2\mathbb{N}}{\Re}\mathbf{O} + \frac{2\mathbb{N}^2}{\Re^2}\boldsymbol{\Gamma}$, $\mathbb{N} = (\bar{\mathbf{e}}\cdot\boldsymbol{\Theta})\cdot(\bar{\mathbf{e}}\cdot\boldsymbol{\Lambda})$, $\Re = (\bar{\mathbf{e}}\cdot\boldsymbol{\Theta})\cdot(\bar{\mathbf{e}}\cdot\boldsymbol{\Theta})$, $\boldsymbol{\Theta} = \frac{\partial\bar{\mathbf{S}}}{\partial\xi}$, $\boldsymbol{\Lambda} = \frac{\partial^2\bar{\mathbf{S}}}{\partial\xi^2}$, $C_{ij} = \Lambda_c\Lambda_d$, $O_{ij} = \Theta_c\Lambda_d + \Theta_d\Lambda_c$ and $\Gamma_{ij} = \Theta_c\Theta_d$. Here, the subscripts are $i = 3(d-1)+t$, $j = 3(c-1)+t$, $c = 1$–4, $d = 1$–4, $t = 1$–3.

Accordingly, the formulation for the Jacobian of the elastic forces associated with the bending strain energy of the beam element can be written as

$$\begin{aligned}\mathbf{J}^{\kappa} = \frac{EI}{2}\int_l \frac{1}{|(\mathbf{r}_0)_\xi|^4}\Bigg[&(\bar{\kappa}-\bar{\kappa}_0)\\ &\times\left(-\frac{1}{2\bar{\kappa}^3}\frac{\partial\bar{\kappa}^2}{\partial\mathbf{e}}\frac{\partial\bar{\kappa}^2}{\partial\mathbf{e}} + \frac{1}{\bar{\kappa}}\frac{\partial^2\bar{\kappa}^2}{\partial\mathbf{e}^2}\right)\\ &+\frac{1}{2\bar{\kappa}^2}\frac{\partial\bar{\kappa}^2}{\partial\mathbf{e}}\frac{\partial\bar{\kappa}^2}{\partial\mathbf{e}}\Bigg]\mathrm{d}l\\ = \frac{EI}{2}\int_l \frac{1}{|(\mathbf{r}_0)_\xi|^4}\Bigg[&\frac{\bar{\kappa}-\bar{\kappa}_0}{\bar{\kappa}}\\ &\times\left[\boldsymbol{\Psi}_1 - \frac{2}{\Re^3}(\bar{\mathbf{e}}\cdot\boldsymbol{\Psi}_2)(\bar{\mathbf{e}}\cdot\boldsymbol{\Psi}_2)\right]\\ &+\frac{\bar{\kappa}_0}{2\bar{\kappa}^3}(\bar{\mathbf{e}}\cdot\boldsymbol{\Psi}_1)(\bar{\mathbf{e}}\cdot\boldsymbol{\Psi}_1)\Bigg]\mathrm{d}l\end{aligned} \tag{55}$$

where $\boldsymbol{\Psi}_2 = \Re\mathbf{O} - 2\mathbb{N}\boldsymbol{\Gamma}$.

4.2 Formulations for a thin cylindrical shell element of ANCF

Based on the discussion in Sect. 4.1, the elastic forces and their Jacobian of a thin shell element of ANCF can be formulated in a similar way. The elastic forces associated with the mid-surface strain energy can be evaluated by using the computationally efficient method proposed by Liu et al. [9]. Based on Eqs. (42)–(44), the bending strain of the shell element can be further cast as

$$\begin{aligned}U^{\kappa} &= \frac{1}{2}\int_{V_0}\left(\boldsymbol{\epsilon}^{\kappa}\right)^{\mathrm{T}}\mathbf{E}\boldsymbol{\epsilon}^{\kappa}\,\mathrm{d}V_0\\ &= \frac{1}{2}\int_{V_0}(\boldsymbol{\Omega}-\boldsymbol{\Omega}_0)^{\mathrm{T}}\mathbf{E}^{\kappa}(\boldsymbol{\Omega}-\boldsymbol{\Omega}_0)\,\mathrm{d}V_0,\end{aligned} \tag{56}$$

where $\boldsymbol{\Omega} = -z[\,k_{11}\quad k_{22}\quad 2k_{12}\,]^{\mathrm{T}}$, $\boldsymbol{\Omega}_0 = -z[\,(k_0)_{11}\quad (k_0)_{12}\quad 2(k_0)_{22}\,]^{\mathrm{T}}$,

$$\mathbf{E}^{\kappa} = \frac{E}{1-\nu^2}\mathbf{H}^{\mathrm{T}}\begin{bmatrix}1 & \nu & 0\\ \nu & 1 & 0\\ 0 & 0 & \frac{1-\nu}{2}\end{bmatrix}\mathbf{H} \quad \text{and}$$

$$\mathbf{H} = \begin{bmatrix}\frac{1}{a^2} & 0 & 0\\ \frac{\cot^2(\theta)}{a^2} & \frac{\csc^2(\theta)}{b^2} & -\frac{\cot(\theta)\csc(\theta)}{ab}\\ -\frac{2\cot(\theta)}{a^2} & 0 & \frac{\csc(\theta)}{ab}\end{bmatrix}.$$

The entries in vector $\boldsymbol{\Omega}$ have been given in Eq. (43).

The elastic forces associated with the bending strain energy of the shell element can be expressed by

$$\mathbf{Q}^{\kappa} = \frac{\partial U^k}{\partial\mathbf{e}} = \int_{V_0}(\boldsymbol{\Omega}-\boldsymbol{\Omega}_0)^{\mathrm{T}}\mathbf{E}^{\kappa}\frac{\partial\boldsymbol{\Omega}}{\partial\mathbf{e}}\,\mathrm{d}V_0. \tag{57}$$

Therefore, the Jacobian of elastic forces associated with the bending strain energy of the shell element can be written as

$$\begin{aligned}\mathbf{J}^{\kappa} = \frac{\partial\mathbf{Q}^{\kappa}}{\partial\mathbf{e}} &= \int_{V_0}\frac{\partial\boldsymbol{\Omega}^{\mathrm{T}}}{\partial\mathbf{e}}\mathbf{E}^{\kappa}\frac{\partial\boldsymbol{\Omega}}{\partial\mathbf{e}}\,\mathrm{d}V_0\\ &\quad -\int_{V_0}(\boldsymbol{\Omega}-\boldsymbol{\Omega}_0)^{\mathrm{T}}\mathbf{E}^{\kappa}\frac{\partial^2\boldsymbol{\Omega}}{\partial\mathbf{e}^2}\,\mathrm{d}V_0.\end{aligned} \tag{58}$$

As can be seen from Eqs. (57) and (58), the terms $\frac{\partial\boldsymbol{\Omega}}{\partial\mathbf{e}}$ and $\frac{\partial^2\boldsymbol{\Omega}}{\partial\mathbf{e}^2}$ should be evaluated to determine the elastic forces and their Jacobian. From Eq. (56), thus, the two partial derivative terms $\frac{\partial\kappa_{\alpha\beta}}{\partial\mathbf{e}}$ and $\frac{\partial^2\kappa_{\alpha\beta}}{\partial^2\mathbf{e}}$ ($\kappa_{\alpha\beta}$ denotes the entries in vector $\boldsymbol{\Omega}$, $\alpha = 1, 2$ and $\beta = 1, 2$) should be calculated. After some complicated mathematical manipulations, the term $\frac{\partial\kappa_{\alpha\beta}}{\partial\mathbf{e}}$ can be directly expressed in terms of their components as following:

$$\begin{aligned}&\frac{\partial\kappa_{\alpha\beta}}{\partial\mathbf{e}}\\ &= \frac{\partial[\frac{\bar{e}_{as}(\bar{\mathbf{S}}_{,\alpha\beta})_s t_a}{\|\mathbf{t}\|}]}{\partial\mathbf{e}}\\ &= \frac{\|\mathbf{t}\|^2\frac{\partial\bar{e}_{as}}{\partial\mathbf{e}}(\bar{\mathbf{S}}_{,\alpha\beta})_s t_a + \frac{\partial\bar{n}_f}{\partial\mathbf{e}}(\|\mathbf{t}\|^2\bar{e}_{fs}(\bar{\mathbf{S}}_{,\alpha\beta})_s - \bar{e}_{as}(\bar{\mathbf{S}}_{,\alpha\beta})_s t_a t_f)}{\|\mathbf{t}\|^3},\end{aligned} \tag{59}$$

where, similarly to Eq. (50), $\bar{\mathbf{S}}$ and $\bar{\mathbf{e}}$ are respectively the transformed shape function and the nodal coordinates of the shell element; $\bar{\mathbf{S}}_{,\alpha\beta}$ denotes the partial derivative of $\bar{\mathbf{S}}$ with respect to η and ξ (for example: $\bar{\mathbf{S}}_{,12} = \frac{\partial^2 \bar{\mathbf{S}}}{\partial \xi \partial \eta}$), and $\mathbf{t} = \mathbf{r}_\xi \times \mathbf{r}_\eta$. The other subscripts in Eq. (59) are $f = 1$–3, $s = 1$–12 and $a = 1$–3.

The formulation for evaluating $\frac{\partial^2 \kappa_{\alpha\beta}}{\partial^2 \mathbf{e}}$ can be written as

$$\frac{\partial^2 \kappa_{\alpha\beta}}{\partial^2 \mathbf{e}} = \frac{\boldsymbol{\Delta}_{,\alpha\beta} + (\boldsymbol{\Delta}_{,\alpha\beta})^{\mathrm{T}} + (\|\mathbf{t}\|^2 \bar{e}_{as}(\bar{\mathbf{S}}_{,\alpha\beta})_s - \bar{n}_f \bar{e}_{fs}(\bar{\mathbf{S}}_{,\alpha\beta})_s t_a) \frac{\partial^2 t_a}{\partial \mathbf{e}^2} - \bar{e}_{as}(\bar{\mathbf{S}}_{,\alpha\beta})_s t_a \frac{\partial t_f}{\partial \mathbf{e}} \frac{\partial t_f}{\partial \mathbf{e}}}{\|\mathbf{t}\|^3}, \tag{60}$$

in which

$$\boldsymbol{\Delta}_{,\alpha\beta} = (\bar{\mathbf{S}}_{,\alpha\beta})_s \left[\|\mathbf{t}\|^2 \frac{\partial t_a}{\partial \mathbf{e}} \frac{\partial \bar{e}_{as}}{\partial \mathbf{e}} - t_f \frac{\partial t_f}{\partial \mathbf{e}} t_a \frac{\partial \bar{e}_{as}}{\partial \mathbf{e}} \right] + \frac{\partial t_f}{\partial \mathbf{e}} t_f \frac{\partial t_a}{\partial \mathbf{e}} \left[\frac{3}{2\|\mathbf{t}\|^2} t_h t_{hs} (\bar{\mathbf{S}}_{,\alpha\beta})_s t_a - \bar{e}_{as}(\bar{\mathbf{S}}_{,\alpha\beta})_s \right], \quad h = 1\text{–}3,$$

$$\frac{\partial t_k}{\partial \mathbf{e}} = \frac{\partial \bar{e}_{md}(\bar{\mathbf{S}}_{,\xi})_d}{\partial \mathbf{e}} \times \bar{e}_{nb}(\bar{\mathbf{S}}_{,\eta})_b + \bar{e}_{md}(\bar{\mathbf{S}}_{,\xi})_d \times \frac{\partial \bar{e}_{nb}(\bar{\mathbf{S}}_{,\eta})_b}{\partial \mathbf{e}} = \epsilon_{mnk} (\mathbf{L} - \mathbf{L}^{\mathrm{T}})_{db} \bar{e}_{nb} \frac{\partial \bar{e}_{md}}{\partial \mathbf{e}}, \tag{61}$$

and

$$\frac{\partial^2 t_k}{\partial e_i \partial e_j} = \epsilon_{mnk} \frac{\partial \bar{e}_{md}}{\partial e_i} \frac{\partial \bar{e}_{nb}}{\partial e_j} \left(\mathbf{L} - \mathbf{L}^{\mathrm{T}} \right)_{db}, \tag{62}$$

where $\mathbf{L} = \bar{\mathbf{S}}_{,\xi} \bar{\mathbf{S}}_{,\eta}$ denotes the dyadic product of $\bar{\mathbf{S}}_{,\xi}$ and $\bar{\mathbf{S}}_{,\eta}$, and the other subscripts in Eqs. (61) and (62) are $i = 1$–36, $j = 1$–36, $d = 1$–12, $b = 1$–12, $m = 1$–3, $n = 1$–3 and $k = 1$–3.

Finally, the elastic forces and their Jacobian of the shell element can be obtained by substituting Eqs. (59)–(62) into Eqs. (57) and (58).

5 Computation strategy

The assembly of the finite elements of ANCF can be carried out in a similar way of traditional finite element method. The nodal coordinate $\mathbf{e}$ of a finite element can be easily transformed into the generalized coordinate $\mathbf{q}$ of the flexible multibody system. Based on ANCF, the final dynamic equations for a constrained rigid-flexible multibody system can be expressed in a compact form as a set of differential algebraic equations with a constant mass matrix as following [24, 25]:

$$\begin{cases} \mathbf{M}\ddot{\mathbf{q}} + \boldsymbol{\Phi}_{\mathbf{q}}^{\mathrm{T}} \boldsymbol{\lambda} + \mathbf{F}(\mathbf{q}) = \mathbf{Q}(\mathbf{q}) \\ \boldsymbol{\Phi}(\mathbf{q}, t) = \mathbf{0}, \end{cases} \tag{63}$$

where $\mathbf{M}$ is the constant mass matrix of the system, $\mathbf{F}(\mathbf{q})$ is the elastic force vector, which is a nonlinear function of nodal coordinates, $\boldsymbol{\Phi}(\mathbf{q}, t)$ represents the vector that contains the system constraint equations, $\boldsymbol{\Phi}_{\mathbf{q}}$ is the derivative matrix of constraint equations with respect to the generalized coordinates $\mathbf{q}$, $\boldsymbol{\lambda}$ is the Lagrange multiplier, $\mathbf{Q}(\mathbf{q})$ is the external generalized forces, which can be obtained by using the principle of virtual work.

Many numerical integration methods have been proposed so far for solving Eq. (63) [26–29]. In this work, the generalized-alpha method [30, 31] is used so as to achieve an optimal combination of accuracy at the low-frequency range and numerical damping at the high-frequency range. Such a method has exhibited good applicability to even more tough problems in the works by Tian et al. [32, 33] and by Liu et al. [34] to study the dynamics of flexible multibody system with clearance joints.

6 Case studies and discussion

6.1 Static test of a thin parallelogram plate

This subsection demonstrates that the thin cylindrical shell element of ANCF is applicable to a thin parallelogram plate clamped to the ground as shown in Fig. 6, where the plate is subject to two concentrated forces at points B and C. The length L, the width W and the thickness of the plate are set to be 0.5, 0.15 and 0.001 m, respectively. The angle θ between the

Table 1 The plate displacement of point C in three directions

Element type (number of elements)	X-displacement (m)	Y-displacement (m)	Z-displacement (m)
ANCF (10×3 elements)	-8.599×10^{-2}	1.498×10^{-2}	2.572×10^{-1}
ANCF (20×6 elements)	-9.251×10^{-2}	1.184×10^{-2}	2.681×10^{-1}
ANCF (50×15 elements)	-9.308×10^{-2}	1.146×10^{-2}	2.691×10^{-1}
ABAQUS (20×6 elements)	-9.305×10^{-2}	1.143×10^{-2}	2.691×10^{-1}
ABAQUS (50×15 elements)	-9.308×10^{-2}	1.146×10^{-2}	2.691×10^{-1}

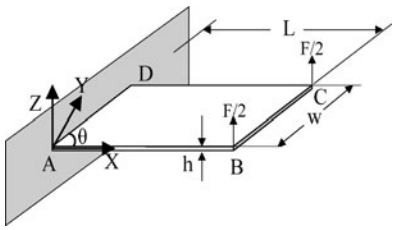

Fig. 6 Initial configuration of a thin cantilever parallelogram plate subjected to two concentrated forces

edges AB and CD is assumed to yield the conditions: $\sin(\theta) = 0.8$ and $\cos(\theta) = 0.6$. The Young's modulus of plate material is set to 2.07×10^{11} Pa. The applied concentrated force F is set to 20 N. For comparison, the same problem is also computed by using a licensed commercial software ABAQUS.

Table 1 lists the computational results of the plate displacement of point C in three directions while different shell elements are used. The table shows that the numerical results of the thin shell elements of ANCF will converge to those of ABAQUS with an increase of the number of shell elements.

6.2 Bending tests of an initially-curved cantilever beam and a cantilever cylindrical shell

This subsection first presents the case study of an initially-curved cantilever beam with square cross section subject to a concentrated bending moment at its free end. The initial configuration of the beam is assumed to be a half-circle with a radius 0.5 m. For numerical comparison, according to [35], the concentrated bending moment acting at its free end is set to $\lambda \pi EI/l$. The ratio of the beam height to beam length (h/L) is set to 0.022. The Young's modulus of beam material is set to 2.1×10^{10} Pa, and the Poisson's ratio is assumed to be zero so as to avoid locking problem. The similar planar model has been studied

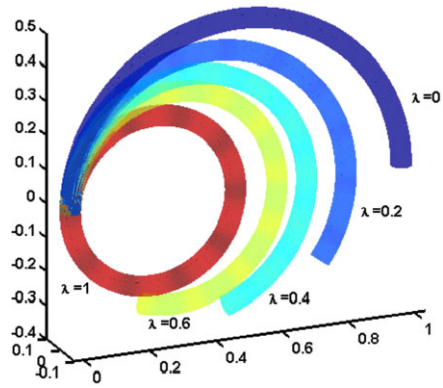

Fig. 7 The bending test of an initially-semicircle cantilever beam

by Sugiyama et al. [13] and Gerstmayr et al. [15]. In this study, the beam is modeled by using 10 spatial curved slender-beam elements of ANCF presented in Sect. 2. The simple way of imposing the concentrated moment on the finite elements of ANCF proposed by Liu et al. [36] is adopted in the present work. The final configuration of the initially curved cantilever beam approximates a full circle when $\lambda = 1$. Figure 7 shows five different beam configurations under specific concentrated moments at its free end. Besides, the final configuration of the cantilever beam just approximates a full circle due to the strong coupling between the axial strain and the bending strain of the element [15].

Furthermore, the subsection turns to the bending problem of an initially-semicircle cantilever shell. The initial radius of the shell is set to 0.5 m. The width and thickness of the shell are 0.5 and 0.001 m, respectively. The Young's modulus of shell material is set to 2.07×10^{11} Pa, and the Poisson's ratio is also assumed to be zero in order to avoid the Poisson locking. The external distribution moment applied at the free edge of the shell is $\lambda \pi EI/(wl)$. Here, w denotes the shell width and l denotes the shell length. The cantilever shell is modeled by using 30×6 thin shell elements

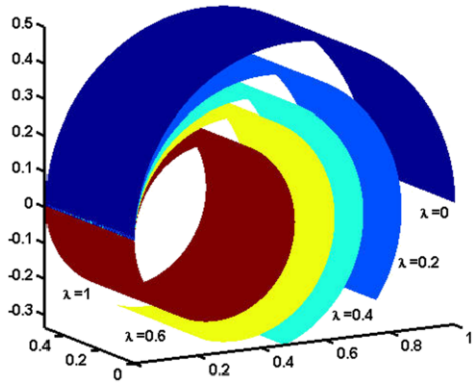

Fig. 8 The bending test of an initially-semicircle cantilever shell

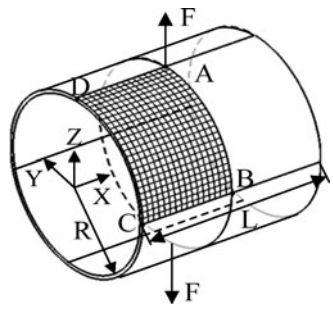

Fig. 9 Initial configuration of a pinched cylinder

of ANCF presented in Sect. 3. Figure 8 shows five different shell configurations under specific distribution moments at its free edge. The final configuration of the shell will also approximate a full circle when $\lambda = 1$.

6.3 Pinched cylinder with free edges

This subsection presents a classical benchmark test for the cylindrical shell element as studied in previous works [37, 38]. As shown in Fig. 9, a free cylindrical shell is subjected to a pair of opposite forces at the midpoint of the top and bottom surfaces. As suggested in previous studies, the length L of the cylindrical shell is set to 10.35 mm, and the inner radius R and the thickness are 4.953 and 0.094 mm, respectively. Both forces applied on the shell are 40 kN. The elastic material properties are represented by the Young's modulus $E = 10.5 \times 10^6$ N/mm^2 and Poisson's ratio $\nu = 0.3125$. As a consequence, the obtained results are compared with those in the previous literature [37, 38].

Because of the geometric symmetry, only one upper quarter of the whole shell needs to be studied. To

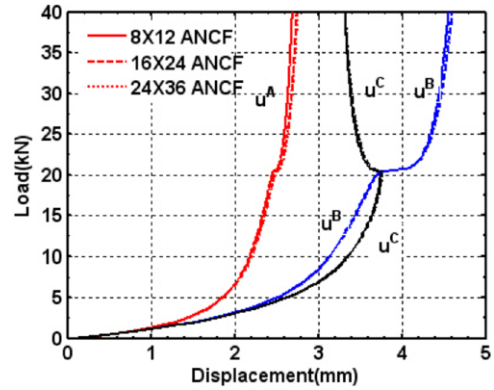

Fig. 10 Magnitudes of displacements at nodes A, B and C

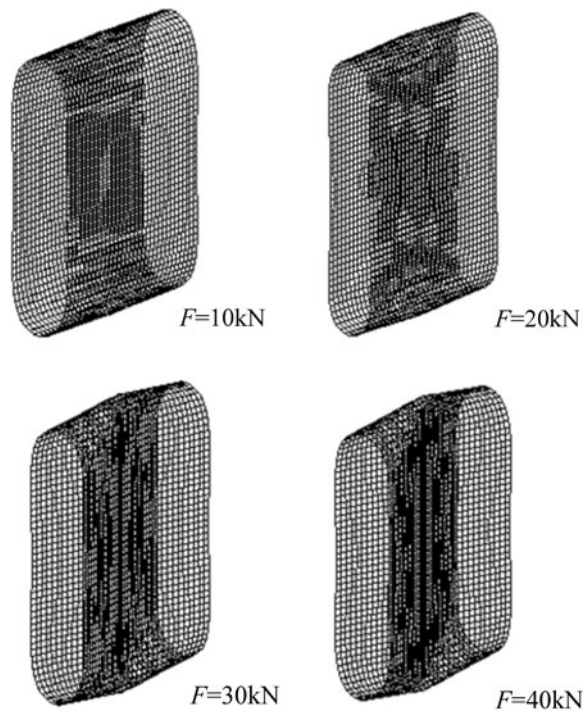

Fig. 11 Deformed configurations of the cylinder shell under pulling forces

display the deformation process in detail, 100 equidistant time increments are applied, and the adopted error tolerance is set to 1.0×10^{-6}. Figure 10 shows the magnitudes of displacements at nodes A, B and C with 8×12, 16×24 and 24×36 elements. The figure indicates that 16×24 shell elements are enough to obtain convergent results. The results are in good agreement with those in the work by Schwarze and Reese [37].

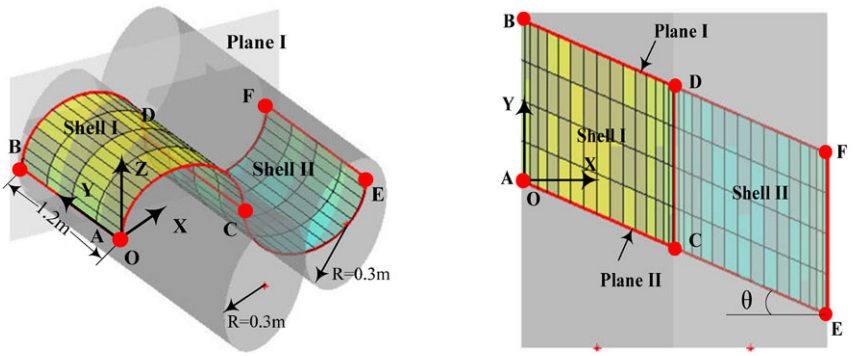

(a) Overall view of the double pendulum **(b)** Top view of the double pendulum

Fig. 12 A spatial double pendulum composed of two parts of cylindrical shells

From the displacements of point B and C, it is obvious that the response of the cylindrical shell exhibits two different stages. The beginning of deformation process is dominated by bending with a large displacement. Subsequently, when the loads are approximate to $F = 20$ kN, the displacement of the shell is characterized by a very stiff response. Figure 11 depicts the four different deformed configurations of the cylindrical shell subjected to $F = 10, 20, 30, 40$ kN, respectively.

6.4 Dynamics of a double pendulum composed of two parts of cylindrical shells

The final case is to study the dynamics of a double pendulum composed of two parts of thin cylindrical shells. As shown in Fig. 12, the two curved parts come from two cylindrical shells trimmed by two parallel cutting planes I and II. The angle θ between a cutting plane and the plane O–X–Z in global coordinate frame yields $\tan(\theta) = 0.5$. The diameters of the cylindrical shells are both 0.3 m. As shown in Fig. 12(b), the generatrices of these two cylindrical shells are both parallel with the direction of Y-axis of global coordinate frame. The Young's modulus of shell material is assumed to be 1.0×10^9 Pa, material density is 7810 kg/m^3. The thickness of the cylindrical shell is set to 0.01 m. As shown in Fig. 12(a), the edge AB of the shell I is fixed on the ground, and its length is set to 1.2 m. Shell I and shell II are connected by the cylindrical joint along the edge CD. The gravitational acceleration is chosen as 9.81 m/s^2.

An objective of this case study is to check the influence of the number of thin shell elements of ANCF on the system dynamic responses. As shown in Fig. 13, the difference of the pendulum displacement of point F in Z-direction becomes smaller and smaller with an increase of the number of finite elements. Figure 13 indicates that 24×16 shell elements are enough to give convergent results. Figure 14 shows the dynamic

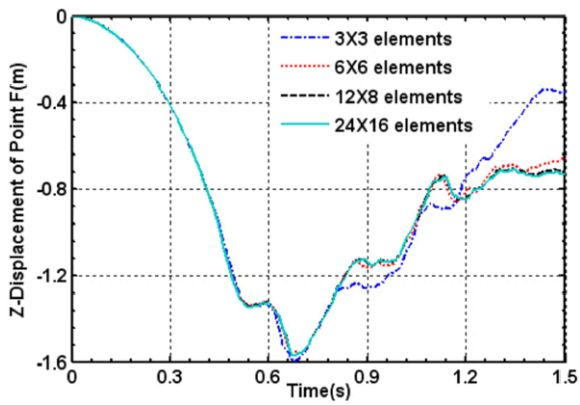

Fig. 13 Pendulum displacement of point F in Z-direction computed by using different number of finite elements

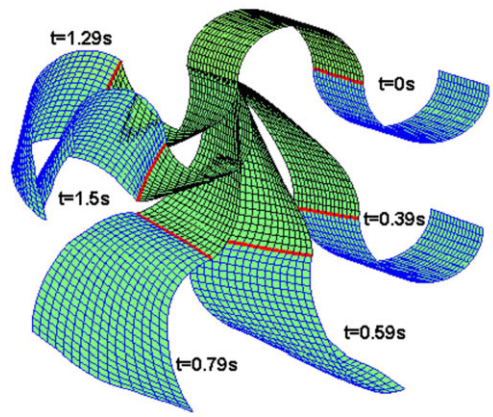

Fig. 14 Dynamic configurations of the double pendulum

Table 2 The CPU time for the models with different number of elements

Number of elements of each cylindrical shell	3×3	6×6	12×8	24×16
The CPU time, seconds	39	162	528	3349

configuration of the system with respect to six specific moments.

All the above numerical simulations are performed on a workstation with 12 processors of 3.33 GHz and a RAM of 96 GB. Table 2 shows the computational time required for different systems. In the process of simulation, the integration step is set to 5×10^{-4} s. From Table 2, the effect of the number of the finite elements on the computational efficiency is significant, and the cost of computational time is almost proportional to the number of finite elements.

7 Conclusions

A new spatial curved slender-beam finite element and a new thin cylindrical shell finite element are proposed in the frame of gradient-deficient ANCF. The longitudinal strain energy for the spatial curved slender-beam element is derived by using the definition of Green–Lagrange strain tensor in continuum mechanics, while the bending strain energy is deducted with help of a local Frenet coordinate frame of the beam axis. The assumption on small strains can be relaxed in the final strain energy formulation. By using similar procedures, the strain energy for the cylindrical shell element is also derived. By defining a local curved surface coordinate frame and a Cartesian coordinate frame, the angle between two base vectors of the defined surface coordinate frame is introduced into the finial strain energy formulations for the shell element. Therefore, the shell element can be used to model the parallelogram shells. To efficiently solving the system equations, the analytical formulations of elastic forces and their Jacobian of the two finite elements of gradient-deficient ANCF are derived. The generalized-alpha method with controllable numerical dissipation is used to solve the huge set of system equations. Finally, the validation and performance of the two finite elements of gradient-deficient ANCF are illustrated by four numerical case studies including both static and dynamic problems. In future research, the proposed method will be applied to study the spherical shell element based on ANCF. Furthermore, the model of wrinkle/slack mechanics can be introduced into the thin shell element of gradient-deficient ANCF in order to study the complex dynamic behaviors of the large scale space structures with very soft thin membranes, such as the solar sails.

Acknowledgements The authors express their sincere thanks to Prof. Daniel García-Vallejo from University of Seville, Spain, and Dr. Johannes Gerstmayr from Johannes Kepler University of Linz, Austria, for the valuable suggestions to the study of ANCF. They also appreciate the constructive suggestions made by Dr. Paulo Flores from University of Minho, Portugal, to this study. This work was supported in part by National Natural Science Foundations of China under Grant 11002022 and Grant 51075032. The work was also supported in part by Excellent Young Scholar Research Fund from Beijing Institute of Technology.

References

1. Shabana, A.A.: An absolute nodal coordinates formulation for the large rotation and deformation analysis of flexible bodies. Technical report. No. MBS96-1-UIC, University of Illinois at Chicago (1996)
2. Eberhard, P., Schiehlen, W.: Computational dynamics of multibody systems history, formalisms, and applications. J. Comput. Nonlinear Dyn. **1**, 3–12 (2006)
3. Yoo, W.S., Dmitrochenko, O., Yu, D.: Review of finite elements using absolute nodal coordinates for large-deformation problems and matching physical experiments. In: ASME 2005 International Design Engineering Technical Conferences and Computers and Information in Engineering Conference, California, Long Beach (2005). DETC2005-84720
4. Schiehlen, W.: Research trends in multibody system dynamics. Multibody Syst. Dyn. **18**, 3–13 (2007)
5. Shabana, A.A., Yakoub, R.Y.: Three-dimensional absolute nodal coordinate formulation for beam elements: theory. J. Mech. Des. **123**, 606–613 (2001)
6. Yakoub, R.Y., Shabana, A.A.: Three-dimensional absolute nodal coordinate formulation for beam elements: implementation and applications. J. Mech. Des. **123**, 614–621 (2001)
7. Mikkola, A.M., Shabana, A.A.: A non-incremental finite element procedure for the analysis of large deformation of plates and shells in mechanical system applications. Multibody Syst. Dyn. **9**, 283–309 (2003)
8. Omar, M.A., Shabana, A.A.: A two-dimensional shear deformable beam for large rotation and deformation problems. J. Sound Vib. **243**, 565–576 (2001)
9. Liu, C., Tian, Q., Hu, H.H.: Dynamics of large scale rigid-flexible multibody system composed of composite laminated plates. Multibody Syst. Dyn. **26**, 283–305 (2011)

10. Sugiyama, H., Suda, Y.: A curved beam element in the analysis of flexible multibody systems using the absolute nodal coordinates. Proc. Inst. Mech. Eng., Proc., Part K, J. Multi-Body Dyn. **221**, 219–231 (2007)
11. Mikkola, A., Dmitrochenko, O., Matikainen, M.: Inclusion of transverse shear deformation in a beam element based on the absolute nodal coordinate formulation. J. Comput. Nonlinear Dyn. **4**, 1–9 (2009)
12. Shabana, A.A., Maqueda, L.G.: Slope discontinuities in the finite element absolute nodal coordinate formulation: gradient deficient elements. Multibody Syst. Dyn. **20**, 239–249 (2008)
13. Sugiyama, H., Koyama, H., Yamashita, H.: Gradient deficient curved beam element using the absolute nodal coordinate formulation. J. Comput. Nonlinear Dyn. **5**, 021001 (2010)
14. Gerstmayr, J., Shabana, A.A.: Analysis of thin beams and cables using the absolute nodal coordinate formulation. Nonlinear Dyn. **45**, 109–130 (2006)
15. Gerstmayr, J., Irschik, H.: On the correct representation of bending and axial deformation in the absolute nodal coordinate formulation with an elastic line approach. J. Sound Vib. **318**, 461–487 (2008)
16. Berzeri, M., Shabana, A.A.: Development of simple models for the elastic forces in the absolute nodal co-coordinate formulation. J. Sound Vib. **235**, 539–565 (2000)
17. Dmitrochenko, O.N., Pogorelov, D.Y.: Generalization of plate finite elements for absolute nodal coordinate formulation. Multibody Syst. Dyn. **10**, 17–43 (2003)
18. Sanborn, G.G., Choi, J., Choi, J.H.: Curve-induced distortion of polynomial space curves, flat-mapped extension modeling, and their impact on ANCF thin plate finite elements. Multibody Syst. Dyn. **26**, 191–211 (2011)
19. Shabana, A.A.: Computational Continuum Mechanics. Cambridge University Press, Cambridge (2008)
20. Kobayashi, S., Nomizu, K.: Foundations of Differential Geometry, vol. II. Wiley-Interscience, New York (1969)
21. Bronshtein, I.N., Semendyayev, K.A., Musiol, G., Muehlig, H.: Handbook of Mathematics, 5th edn. Springer, Berlin (2007)
22. Gerstmayr, J., Shabana, A.A.: Efficient integration of the elastic forces and thin three-dimensional beam elements in the absolute nodal coordinate formulation. In: Multibody Dynamics 2005 ECCOMAS Thematic Conference, Madrid, Spain, 21–24 June 2005
23. Huang, K.Z., Xue, M.D., Lu, M.W.: Tensor Analysis. Tsinghua University Press, Beijing (2003) (in Chinese)
24. Shabana, A.A.: Dynamics of Multibody Systems, 3rd edn. University Press, Cambridge, New York (2005).
25. Shabana, A.A.: Computational Dynamics, 3rd edn. Wiley, New York (2010)
26. Hussein, B., Negrut, D., Shabana, A.A.: Implicit and explicit integration in the solution of the absolute nodal coordinate differential/algebraic equations. Nonlinear Dyn. **54**, 283–296 (2008)
27. Tian, Q., Zhang, Y., Chen, L., Yang, J.: An efficient hybrid method for multibody dynamics simulation based on absolute nodal coordinate formulation. J. Comput. Nonlinear Dyn. **4**, 021009 (2009)
28. Shabana, A.A., Hussein, B.: A two-loop sparse matrix numerical integration procedure for the solution of differential/algebraic equations: application to multibody systems. J. Sound Vib. **327**, 557–563 (2009)
29. Hussein, B., Shabana, A.A.: Sparse matrix implicit numerical integration of the stiff differential/algebraic equation: implementation. Nonlinear Dyn. **65**, 369–382 (2011)
30. Chung, J., Hulbert, G.: A time integration algorithm for structural dynamics with improved numerical dissipation: the generalized-alpha method. J. Appl. Mech. **60**, 371–375 (1993)
31. Arnold, M., Brüls, O.: Convergence of the generalized-alpha scheme for constrained mechanical systems. Multibody Syst. Dyn. **18**, 185–202 (2007)
32. Tian, Q., Zhang, Y., Chen, L., Yang, J.: Simulation of planar flexible multibody systems with clearance and lubricated revolute joints. Nonlinear Dyn. **60**, 489–511 (2010)
33. Tian, Q., Liu, C., Machado, M., Flores, P.: A new model for dry and lubricated cylindrical joints with clearance in spatial flexible multibody systems. Nonlinear Dyn. **64**, 25–67 (2011)
34. Liu, C., Tian, Q., Hu, H.H.: Dynamics and control of a spatial rigid-flexible multibody system with multiple cylindrical clearance joints. Mech. Mach. Theory **52**, 106–129 (2012)
35. Timoshenko, S., Gere, J.: Mechanics of Materials. Van Nostrand Reinhold, New York (1972)
36. Liu, C., Tian, Q., Hu, H.H., García-Vallejo, D.: Simple formulations of imposing moments and evaluating joint reaction forces for rigid-flexible multibody systems. Nonlinear Dyn. **69**, 127–147 (2012)
37. Schwarze, M., Reese, S.: A reduced integration solid-shell finite element based on the EAS and the ANS concept-large deformation problems. Int. J. Numer. Methods Eng. **85**, 289–329 (2010)
38. Arciniega, R.A., Reddy, J.N.: Tensor-based finite element formulation for geometrically nonlinear analysis of shell structures. Comput. Methods Appl. Mech. Eng. **196**, 1048–1073 (2007)